Systematic study of terahertz response of $SrTiO_3$ based heterostructures: Influence of strain, temperature, and electric field

V. Skoromets,[1] C. Kadlec,[1] J. Drahokoupil,[1] J. Schubert,[2] J. Hlinka,[1] and P. Kužel[1,*]

[1]*Institute of Physics, Academy of Sciences of the Czech Republic, Na Slovance 2, CZ-18221 Prague 8, Czech Republic*

[2]*Peter Gruenberg Institute, PGI 9-IT, JARA-FIT, Research Centre Juelich, D-52425 Juelich, Germany*

(Received 14 March 2014; revised manuscript received 6 June 2014; published 30 June 2014)

Epitaxial heterostructures consisting of a variable number of $SrTiO_3/DyScO_3$ bilayers deposited on $DyScO_3$ substrates were investigated using time-domain terahertz spectroscopy down to helium temperatures. Interdigitated electrodes deposited on top of the structures allowed probing of the terahertz response upon an applied electric field. The phase transition into a ferroelectric state is observed in $SrTiO_3$ films in all samples close to room temperature (between 250 and 310 K) due to in-plane epitaxial strain induced by the substrate and intercalated layers of $DyScO_3$. Evolution of the dielectric spectra with temperature and external electric field is described by a general model which involves a damped harmonic oscillator (soft mode) coupled to a Debye relaxation (central mode). Both modes are connected with the soft mode eigenvector, as recently shown by molecular dynamics simulations, and they reflect a strong anharmonicity of the soft-mode potential. At high temperatures the soft-mode frequency variation drives all the changes observed in the spectra with temperature and applied field. At low temperatures, deep in the ferroelectric phase, the soft mode significantly hardens and loses its importance for the terahertz dynamics; the central mode becomes stronger and it almost completely determines the shape of the measured spectra. The observed variation of phase transition temperature and of the dielectric response among the structures is ascribed to a partial epitaxial strain relaxation confirmed also by x-ray diffraction.

DOI: 10.1103/PhysRevB.89.214116 PACS number(s): 77.55.fp, 77.22.Ch, 77.55.Px

I. INTRODUCTION

Ferroelectric materials are characterized by a high permittivity value up to the far infrared range given by a strongly polar low-frequency (soft) phonon and/or polar relaxations. The soft vibrational mode which triggers the ferroelectric phase transition is a characteristic spectroscopic feature of displacive ferroelectrics [1]. Strontium titanate ($SrTiO_3$, STO) is an example of a typical displacive incipient ferroelectric material. Its low-frequency dielectric properties are almost entirely governed by the dynamics of the ferroelectric soft mode. The contribution of the soft mode to the low-frequency permittivity is dominant due to its very low frequency ω_0 and strongly polar character,

$$\Delta\varepsilon = \frac{f}{\omega_0^2}, \tag{1}$$

where f is the oscillator strength proportional to the square of the effective charge associated with the soft-mode eigenvector. In a single crystal the soft-mode frequency decreases upon cooling, leading to the increase of the permittivity value. At the same time the material remains in the paraelectric phase down to the lowest temperatures due to quantum fluctuations [2].

The strongly anharmonic character of the soft mode along with its large effective charge provides a possibility of permittivity tuning by means of an external electric field. Indeed, STO has been extensively studied in view of its applications in microwave tunable devices [3,4]. However, these investigations were mostly limited to low temperatures (below 100 K), and it was commonly accepted that STO crystals are not tunable above ~100 K. Recently, an electric-field tunability of the terahertz dielectric properties of STO single crystals has been observed up to room temperature and quantitatively related to the soft-mode anharmonic coefficient [5]. Naturally, high-temperature tunability of STO crystals is rather weak. The ways to increase the room-temperature tunability of STO-based structures are based on the idea of inducing the ferroelectric phase transition in the material near room temperature. This can be achieved by chemical substitution of strontium by barium ($Ba_xSr_{1-x}TiO_3$ solid solutions) [6] or by tensile strain introduced during the epitaxial growth of STO thin films on appropriate substrates [7]. The latter possibility has been extensively investigated during the past years in several $SrTiO_3/DyScO_3$ thin films and multilayers [8–12]. Thin STO films grown on (110)-oriented $DyScO_3$ (DSO) substrates are of particular interest because the ferroelectric phase transition occurring near ~300 K [7] leads to a highly enhanced dielectric tunability at room temperature.

It is known that the epitaxial strain relaxes with increasing thickness of the STO film. Zhai *et al* [13]. showed that the lattice strain relaxation in STO deposited on DSO occurs mainly at a distance of 50–90 nm from the substrate surface, and for thicknesses larger than 100 nm the surface layer of the film possesses the same lattice constants as those of a freestanding crystal.

In this paper we present a comprehensive analysis of terahertz dielectric properties of thin-film structures consisting of STO and DSO layers and we explore the possibility to increase the total thickness of strained STO films while maintaining their strain-induced dielectric properties. The prepared multilayer structures consist of a variable number of STO/DSO bilayers, where the DSO layers are intended to maintain the epitaxial strain in STO films at larger distances

*Author to whom correspondence should be addressed: kuzelp@fzu.cz

from the substrate. The dielectric response of the structures at various temperatures (20–294 K) and applied electric fields (0–93 kV/cm) is studied using time-domain terahertz spectroscopy. The degree of epitaxial strain relaxation is investigated in several thin-film heterostructures by x-ray diffraction (XRD). We provide a comparison of the most important parameters describing lattice dynamics in each studied structure.

II. EXPERIMENTAL DETAILS

Thin-film structures were prepared by pulsed laser deposition (PLD) on (110)-oriented $10 \times 10 \times 0.9$ mm^3 DSO substrates. The deposition was performed in on-axis geometry using a KrF excimer laser. An STO single crystal and DSO polycrystal were used as targets. More details about the thin-film deposition technique can be found in Ref. [10]. An interdigitated gold electrode structure was deposited onto each studied heterostructure for application of a bias electric field. The electrode structure covered about one half of the sample surface (see Fig. 1). Metallic electrodes were prepared by lift-off photolithography and subsequent deposition of 20-nm-thick Nb film as the adhesion layer and 300-nm-thick Au film by a dc magnetron sputtering. An active area of the electrode structure consisted of 5-μm-wide gold stripes and of 15-μm-wide gaps. The conducting stripes (electrode fingers) were parallel to the [001] direction of the DSO substrate. The experiments were performed under normal incidence, i.e., the wave vector of the terahertz radiation was perpendicular to the plane of the thin-film structures. The samples were oriented to have the electric-field vector of the probing terahertz radiation perpendicular to the electrode fingers (see Fig. 1). In this experimental arrangement, the terahertz field is polarized along the transparent axis of a birefringent DSO substrate (axis with a lower refractive index and lower losses in the terahertz range).

All investigated samples can be divided in two series. Each series was prepared at once from a preselected set of substrates. Initially, all substrates were polished on both sides to an optical quality and with a precise control of their thickness (± 2 μm) and of their plane parallelism (± 1 μm). Afterwards, all of the DSO substrates were measured using a time-domain terahertz spectrometer in order to estimate their thicknesses as precisely as possible. The next step was the deposition of the thin-film structures. The interdigitated electrode structure was prepared on the samples from the first series (i) just after the thin-film deposition. The room-temperature response of the multilayer structures of this series has already been analyzed and reported in Ref. [10]. The measurement of the temperature dependence of the dielectric properties without bias field and with applied bias field was performed outside the electrode area and inside the active area of the electrodes, respectively. For the second series (ii) of the samples, the temperature dependence of the dielectric properties was measured before the deposition of metallic electrodes. Thus, in this case the same area of the thin-film structure was used for the zero-field measurements (temperature dependence of the permittivity) and for measurements under bias (field-induced changes in the permittivity).

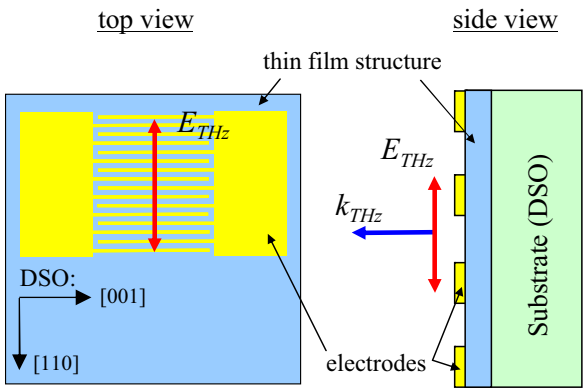

FIG. 1. (Color online) Scheme of the sample geometry and of the orientation of the electric-field vector and wave vector of the incident terahertz radiation.

TABLE I. Investigated thin-film structures. STO/DSO is the number of $SrTiO_3/DyScO_3$ bilayers, d_{layer} is the thickness of individual layers, and d_{STO} is the total thickness of STO layers in each structure.

Sample	1×100	2×50	3×50	4×50A	4×50×2	6×50	8×50
STO/DSO		2	3	4	8	6	8
d_{layer} (nm)	100	50	50	50	50	50	50
d_{STO} (nm)	100	100	150	200	400	300	400

Altogether, seven samples were prepared and fully analyzed in terms of temperature and field dependence of the dielectric properties; their labels and technical descriptions are presented in Table I. Samples 1×100, 2×50, 3×50, and 4×50A are from series (i); the others belong to series (ii). Structure 1×100 is simply a 100-nm-thick single layer of STO film deposited on a DSO substrate. Structures $n \times 50$ consist of n bilayers of STO/DSO, where each single layer of STO or DSO has a thickness of 50 nm. The results obtained for 4×50A sample were already discussed in detail in Ref. [11]; they are included in this paper for completeness of the comparison between different structures. Sample $4 \times 50 \times 2$ consists of identical thin-film structures deposited on both sides of the substrate, and both structures are similar to that of the 4×50A sample. The interdigitated electrodes were subsequently sputtered on one side of the sample only; therefore the total thickness of the STO film taken into account in the field-dependent measurements is 200 nm, while it is 400 nm in the experiments without applied bias. Two additional samples, denoted 4×50B and 4×50C, were prepared with nominally the same structure as sample 4×50A. These samples were involved only in XRD experiments.

A custom-made time-domain terahertz spectrometer powered by a femtosecond laser source (Ti:sapphire oscillator Mira, Coherent) was used for measurements of all the experimental spectra of the thin-film structures. Further details about the experimental setup utilized in this study can be found in Ref. [14]. The spectrometer was equipped with a helium flow cryostat (Optistat, Oxford Instruments), allowing investigation of the samples in a broad temperature range.

The XRD measurements were performed at room temperature using a Panalytical diffractometer X'Pert PRO with Co

tube ($\lambda = 0.178\,9$ nm). We used the parallel beam geometry with a parabolic multilayer mirror in the primary beam and a parallel plate collimator (divergence 0.06°) in the diffracted beam. A texture cradle (ATC-3) allowed us to control inclination and rotation of samples. The lattice parameters were determined from 004 (perpendicular to sample surface), 022, and 222 diffraction maxima in the reciprocal space maps.

III. EXPERIMENTAL RESULTS

A large number of spectra were measured and analyzed in order to characterize all the thin-film structures described above. The measurements were done in two steps. First, equilibrium dielectric properties (without the bias field) of each sample were probed at different temperatures. Second, field-induced dielectric properties were measured at the same set of temperatures.

The time-domain terahertz spectroscopy requires measurements of reference wave forms which normalize the so-called signal wave forms. In the case of the equilibrium measurements (first step), the reference wave forms were measured using a bare DSO substrate, and the signal wave forms were measured using a sample with the thin-film structures. The total optical thickness of STO in any multilayer (<10 μm) is much smaller than the wavelength of terahertz radiation. It can be easily shown, using the transfer matrix formalism [15], that under these conditions, the terahertz transmission through an STO/DSO multilayer is equivalent to that through an STO/DSO bilayer with the same overall thickness of each material. It is then possible to use formulas for a single film (STO with the total thickness) on DSO substrate for the calculation of the STO permittivity. We also verified numerically that this approximation is appropriate.

In the case of measurements with the electric field (second step), the reference wave forms were measured using the sample without an electric bias, whereas the signal wave forms were measured with an applied bias.

A ratio of the Fourier transforms of the signal and reference was calculated for each measurement. In the equilibrium experiments, this ratio provides a complex transmission function $t(\omega)$ of the thin-film structure [10]:

$$t(\omega) = \frac{2N_f(N_s+1)\exp\left[i\omega(N_s-1)\left(d_s-d_s^r\right)/c\right]\exp[i\omega(N_f-1)d_f/c]}{(N_f+1)(N_f+N_s)-(N_f-1)(N_f-N_s)\exp[2i\omega N_f d_f/c]}, \tag{2}$$

where d_f is the film thickness, N_s and N_f are complex refractive indices of the substrate and film, respectively, d_s and d_s^r are thicknesses of the substrate with and without the thin film, respectively, and c is the speed of light in vacuum. The complex refractive index of the thin STO films N_f can be calculated by numerically solving the expression for $t(\omega)$.

In the experiments with an applied electric field, the ratio of the Fourier transforms of the signal and reference t^E reads [10]

$$t^E(\omega) = \frac{N_f^E}{N_f}\frac{(N_f+1)(N_f+N_s)\exp[-i\omega N_f d_f/c]+(1-N_f)(N_f-N_s)\exp[i\omega N_f d_f/c]}{\left(N_f^E+1\right)\left(N_f^E+N_s\right)\exp\left[-i\omega N_f^E d_f/c\right]+\left(1-N_f^E\right)\left(N_f^E-N_s\right)\exp\left[i\omega N_f^E d_f/c\right]}, \tag{3}$$

where N_f^E is the complex refractive index of the STO film under bias, which can be calculated by inverting the expression for $t^E(\omega)$. Some additional details about the experimental spectra evaluation are discussed in Refs. [10] and [11].

The measured equilibrium dielectric spectra of selected samples at three different temperatures are shown in Fig. 2. For other samples the measured spectra are qualitatively similar to those presented in Fig. 2. The permittivity reaches a maximum value of about (or, in some cases, somewhat larger than) 1000 at 10 cm^{-1} close to the room temperature. All loss spectra (Im ε) show rather broad features.

In the second step, i.e., measurements with the electric field, each sample was put into an optical cryostat equipped with wires for the electric field application. Then a set of wave forms was measured under different electric fields applied to the sample at each temperature. In Figs. 3 and 4 we show selected dielectric spectra of two samples for several temperatures and values of the bias electric field. One can observe qualitatively similar electric-field-induced behavior for all the samples, namely, the real part of the low-frequency permittivity (below $\sim$30 cm^{-1}) decreases upon the electric-field application, and the dielectric losses decrease in the whole experimentally achievable spectral range under the bias field. It is clearly seen in Figs. 3 and 4 that the electric-field-induced changes are significantly weaker at temperatures below 200 K than above.

IV. DATA ANALYSIS

A. Model

To interpret the spectra we considered a model involving a pair of linearly coupled lattice modes. A low-frequency excitation ($\sim$10 cm^{-1}) of relaxation type, called a central mode, was observed in the terahertz spectra at room temperature in the previous studies of similar thin-film systems [9,10]. This excitation was not directly coupled to the polarization at room temperature and appeared in the dielectric spectra due to its linear coupling to the ferroelectric soft mode. This behavior was demonstrated [10] in the paraelectric phase of strained STO/DSO structures assigned to the sample series (i) in this paper. This model implies that the appearance and strength of the central mode in the terahertz spectra are strongly correlated with the soft-mode frequency ω_0. Namely, the contribution of the relaxation to the permittivity is negligible if the soft-mode frequency is high (i.e., $\omega_0 \geq 90$ cm^{-1}, as it was found in Ref. [10]), and its contribution is dominating when the soft-mode frequency is low ($\omega_0 \leq 50$ cm^{-1}).

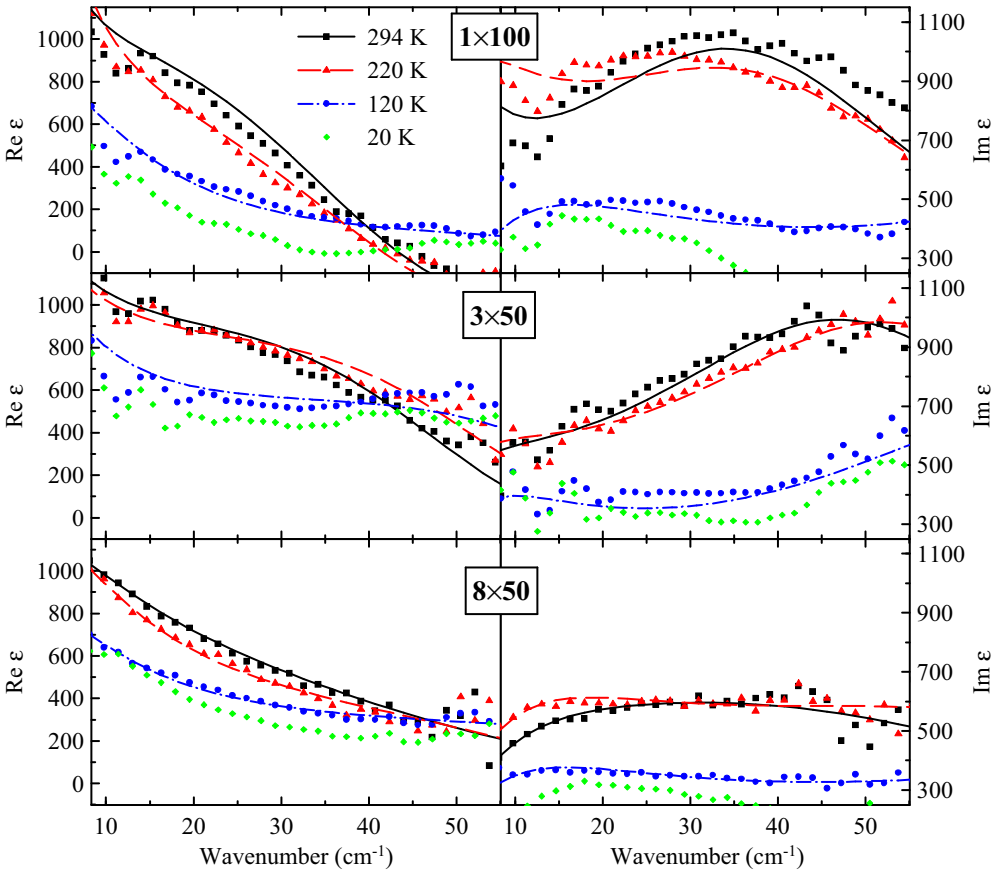

FIG. 2. (Color online) Examples of the measured dielectric spectra for selected thin-film structures at three different temperatures without electric field. Symbols are experimental data; lines are fits with the formula (4). Note the leading contribution of the relaxation mode at low temperatures.

However, at low temperatures in the ferroelectric phase, the relaxation mode is clearly observed in the terahertz spectra even if the soft-mode frequency is high at the same time; this is obvious, for example, in Fig. 4 (curves for 120 K).

Taking into account all these observations, we propose a more general formula [16,17], which has been already applied to the analysis of the terahertz spectra of sample 4×50A [11]:

$$\varepsilon(\omega) = \frac{f(1 - i\omega/\gamma) + g\left(\omega_0^2 - \omega^2 - i\omega\Gamma\right) + 2\delta\sqrt{fg}}{\left(\omega_0^2 - \omega^2 - i\omega\Gamma\right)(1 - i\omega/\gamma) - \delta^2} + \varepsilon_\infty, \tag{4}$$

where the soft mode is modeled by a damped harmonic oscillator with a bare eigenfrequency ω_0, damping Γ, and oscillator strength f, and the central mode is described by a Debye relaxation with frequency γ; δ is a coupling constant and ε_∞ is a contribution of higher-frequency excitations to the permittivity. In this model the bare relaxation mode may contribute directly to the permittivity via its strength g, which denotes dielectric contribution of the bare relaxational mode.

All the dielectric spectra of the investigated samples were fitted by the formula (4). Since this model includes a large number of parameters, it is not possible to determine all of them independently for each spectrum. On the other hand, we measured a very large number of spectra: for each sample spectra are available for about eight temperatures and about 8–10 different bias values were applied for each temperature. This relatively dense mesh of experimental points allows one to determine the main trends in the behavior of various parameters of the fits. Therefore we fixed values of several parameters as independent of temperature (and/or of applied field) and fitted a group of spectra simultaneously. We call this approach a global fit, because values of many parameters are common for all the spectra in the fitted set. Such an approach is not unambiguous; however, it allows us to determine the minimum number of parameters which fit the whole set of spectra and to select the most pertinent ones which control the temperature and field dependence of the spectra. This has implications on our interpretation in terms of the soft-mode behavior. Previous analysis of the spectra for some of the samples at room temperature [10] showed that the relaxation strength in the paraelectric phase vanishes ($g = 0$) while the low-temperature spectra of one of the samples (4×50A) featured an increased contribution of the relaxation mode, which can be taken in to account by a nonvanishing (temperature-dependent) g in the ferroelectric phase [11]. A similar conclusion was drawn also for a thin film of $KTaO_3$ where a ferroelectric phase was induced below 60 K [18].

For each sample a set of global fits was performed as described below.

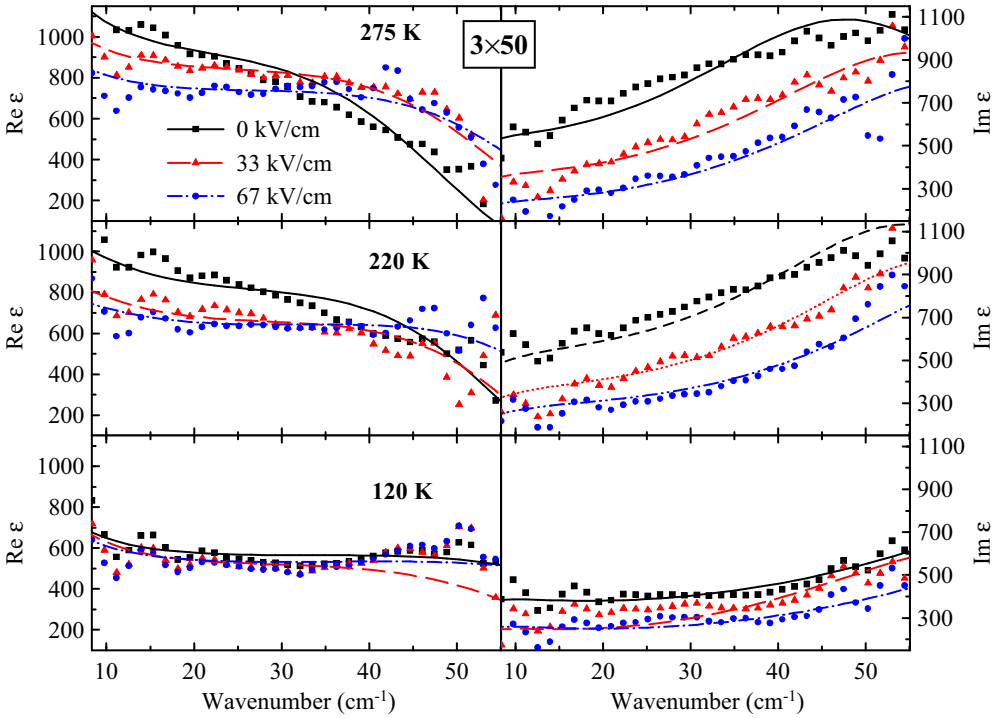

FIG. 3. (Color online) Selected dielectric spectra of sample 3×50 for several temperatures and bias fields. Symbols: experimental data; lines: fits with the formula (4).

B. Temperature dependence

Initially, a global fit of all equilibrium dielectric spectra (all temperatures at zero-bias field) was performed, where we assumed that Γ, f, γ, and δ are temperature independent, and $g(T)$ and $\omega_0(T)$ are temperature dependent. The dependences $g(T)$ and $\omega_0(T)$ are the key results of this part of the data analysis. The temperature evolution of the terahertz dielectric response is entirely described by these temperature-dependent parameters. The high-frequency permittivity ε_∞ was fitted for

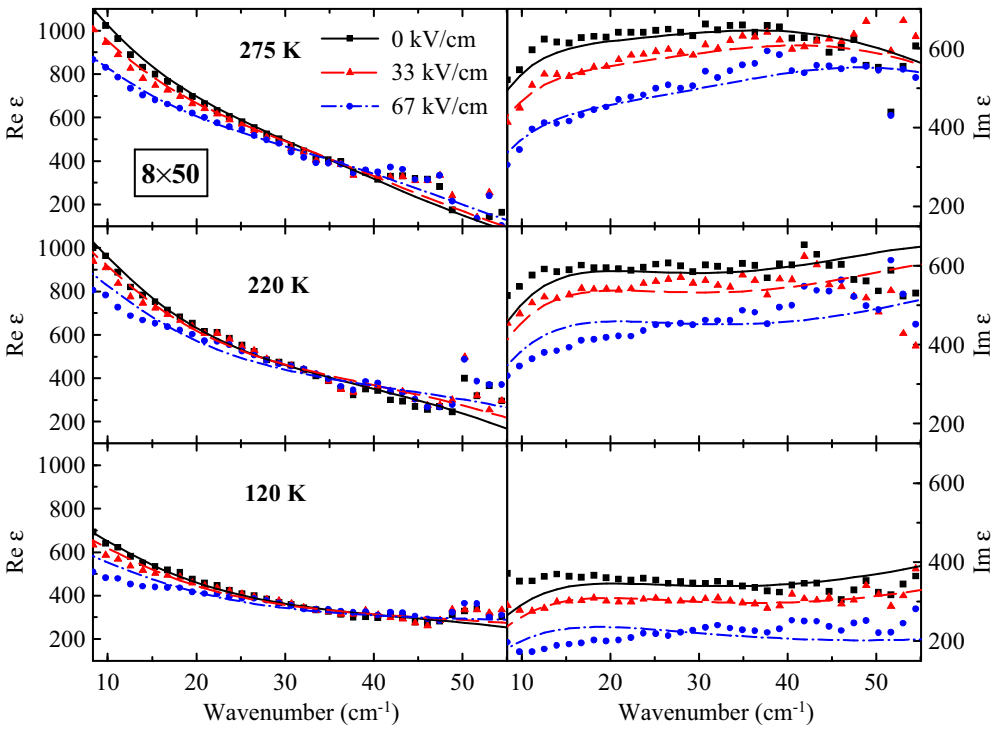

FIG. 4. (Color online) Selected dielectric spectra of sample 8×50 for several temperatures and bias fields. Symbols: experimental data; lines: fits with the formula (4).

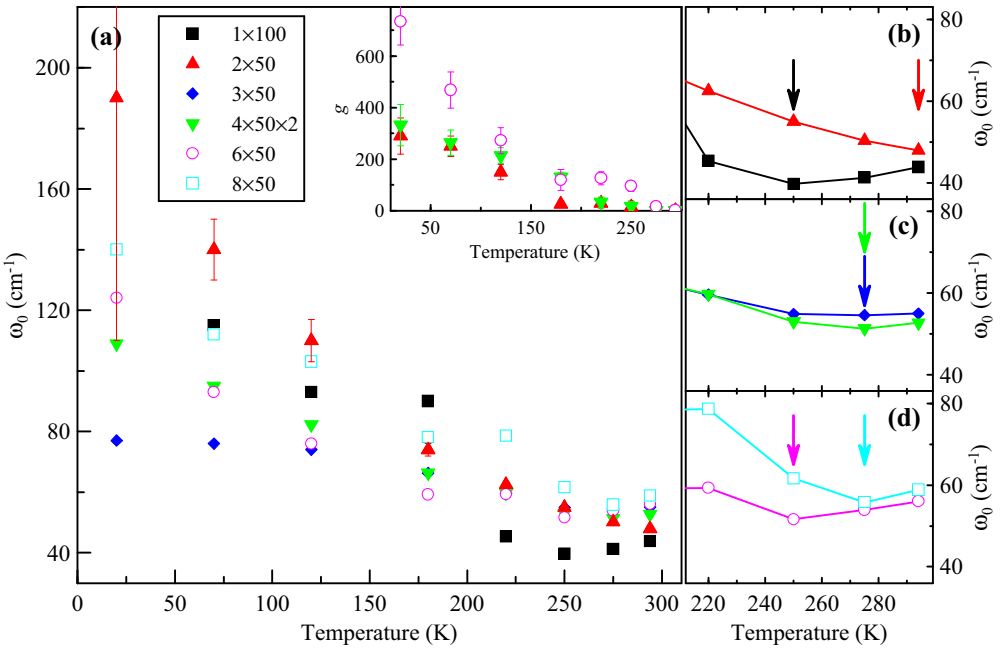

FIG. 5. (Color online) (a) Temperature dependence of the soft-mode frequency as obtained from the fits of the equilibrium spectra of the investigated samples. Inset: temperature dependence of the relaxation strength g for selected samples. (b), (c), (d) The same data shown on an enlarged temperature scale in the vicinity of the phase transition temperature (T_C). Arrows denote the minimum of the soft-mode frequency which is identified with T_C. All values shown in the figure are obtained from the fits with formula (4). The error bars shown in the figure correspond to the errors provided by the global fits; in the case of ω_0 the shown error bars represent typical errors for given values of ω_0.

each spectrum independently. Note that ε_∞ has no physical meaning in our fits, as its value is the subject of a large uncertainty which was discussed in Ref. [10].

The resulting fits for selected thin-film structures are shown along with the measured spectra in Fig. 2. The values of the soft-mode frequency obtained from the fits are presented in Fig. 5. By analyzing the temperature behavior of the soft-mode frequency one can assess the phase transition temperature of each thin-film structure as the temperature where the soft-mode frequency reaches its minimum value. It should be mentioned that the soft-mode frequency provided by the fit at lower temperatures (below 120 K) should be considered as very approximate. The soft-mode frequency is already rather high (above the accessible spectral range), and only its low-frequency tail contributes to the detected part of the spectra. In addition, a high damping of the soft mode leads to its almost constant or weakly frequency-dependent contribution to the permittivity in the experimental spectra. Therefore our model becomes less sensitive to the value of the soft-mode frequency at lower temperatures.

The fits of the equilibrium data showed that the relaxation strength acquires nonzero values only at lower temperatures, namely, when the STO film is in the ferroelectric phase according to the temperature behavior of the soft-mode frequency [see the inset in Fig. 5(a)]. Moreover, $g(T)$ grows with cooling below the transition temperature, i.e., it behaves as a morphic parameter with respect to the phase transition. The 2×50, 3×50, and $4 \times 50 \times 2$ samples exhibit the maximum relaxation strength value of about 300 at 20 K, whereas 1×100, 6×50, and 8×50 show somewhat larger values in the range from 500 to 750. The values of temperature-independent parameters (Γ, δ, f) do not differ much among samples, $\Gamma \approx 50$–$90\ \mathrm{cm}^{-1}$, $\delta \approx 32\ \mathrm{cm}^{-1}$, $f \approx 2.36 \times 10^6\ \mathrm{cm}^{-2}$; the relaxation frequency γ typically acquires values of 7–15 cm^{-1}.

C. Field dependence

In the next step, we fitted an evolution of the dielectric spectra upon an applied electric field. Each set of data for one global fit included spectra obtained for one sample at one temperature under varied bias. Results of such fits along with the experimental data are presented in Figs. 3 and 4 for selected samples and temperatures. In these global fits f was fixed to the value of $2.36 \times 10^6\ \mathrm{cm}^{-2}$ found in the previous fits, which is also in agreement with the value found in STO single crystals [19]; the parameters Γ, δ, and g were fitted independently for each global fit (i.e., for each temperature) in order to compare these values with the previously found values from the measurements without the bias field. Such a crosscheck provides an approximate measure of the robustness of the parameter determination. The coupling constant δ and the oscillator strength g acquired values very close to those obtained from the fits of the equilibrium data with a relative deviation not larger than 15%. The soft-mode damping Γ and the relaxation frequency γ exhibited some nontrivial dependencies, which are discussed below. The key parameter of these fits is, however, the soft-mode frequency $\omega_0(T,E)$, which is the only parameter that was assumed to be electric-field dependent. The complete picture of the soft-mode frequency behavior with temperature and electric field in the 6×50 sample is presented in Fig. 6. The electric-field-induced tuning of ω_0 obtained at 70 and 20 K is not shown because of the low sensitivity of the terahertz spectra to small changes

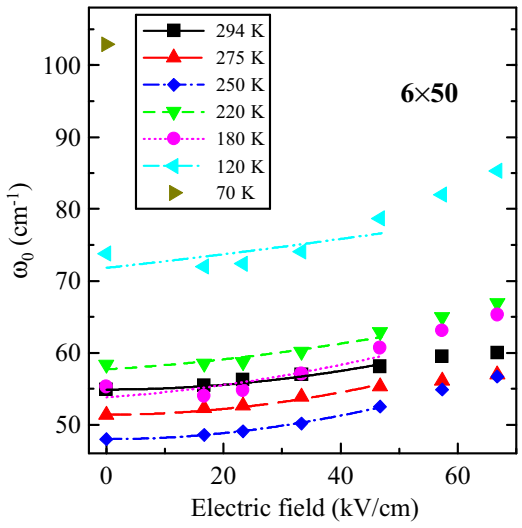

FIG. 6. (Color online) Electric-field-induced tuning of the soft-mode frequency in 6×50 sample. Symbols are the experimental data corresponding to the soft-mode frequency obtained from a fit of experimental spectra by model (4). Lines are fits of $\omega_0(E)$ by expression (5).

in the soft-mode frequency at lower temperatures, as it was discussed above.

V. DISCUSSION

A. Ferroelectric phase transition

From the temperature behavior of the soft-mode frequency shown in Fig. 5 one can conclude that the ferroelectric phase transition occurs at temperatures slightly below room temperature (250–294 K) in all the investigated thin-film structures, with the exception of the 2×50 sample. Its phase transition temperature cannot be rigorously determined because the minimum value of the soft-mode frequency is observed at the edge of the measured temperature range (see Fig. 5). However, taking into account the low value of the soft-mode frequency at room temperature and general trends of the soft-mode temperature behavior for other samples, we can conclude that the transition occurs with a high probability somewhere in the range between 290 and 310 K. The estimated phase transition temperatures, the corresponding frequencies of the soft mode, and the extrapolated values of the static permittivity for all samples are summarized in Table II. It is interesting to note that even though the ferroelectric transition is pushed towards room temperature in the samples investigated here, the overall permittivity is considerably lower than that of the bulk paraelectric STO at low temperatures [20].

The 2×50 structure has the highest observed phase transition temperature. This can be understood by taking into account the fact that the strain distribution is more homogeneous in two separate 50-nm-thick layers of STO than in a 100-nm-thick layer of 1×100 sample; in thicker multilayer systems a gradual reduction of the strain towards the topmost layer can take place.

Indeed, XRD experiments confirm the above statement. Results of these experiments done on five samples and on the

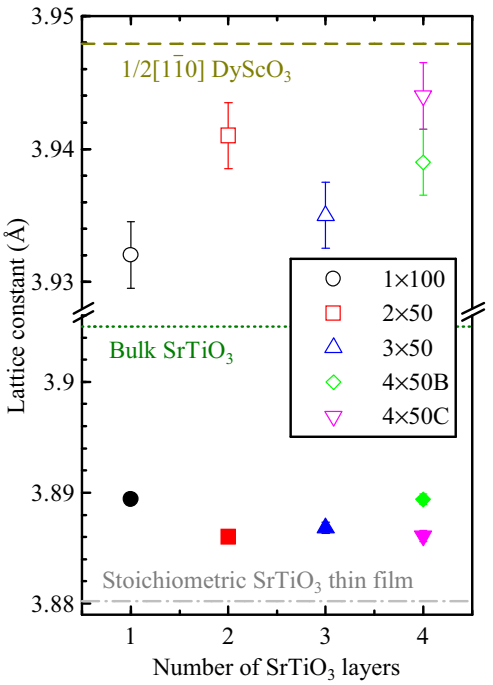

FIG. 7. (Color online) Lattice constants of $SrTiO_3$ as a function of the number of STO layers. Open and solid symbols represent data for the shorter in-plane lattice constant (along [1$\bar{1}$ 0] $DyScO_3$) and for the out-of-plane lattice constant, respectively. The dashed horizontal line corresponds to a shorter constant ½[1$\bar{1}$ 0] of the pseudosquare mesh of (110)-oriented $DyScO_3$ substrate; the value is determined by XRD experiments with the error of ±0.005 Å. The dotted line shows the lattice constant value of a freestanding bulk $SrTiO_3$ crystal. The dash-dotted line corresponds to the out-of-plane lattice constant of a nominally stoichiometric $SrTiO_3$ thin film, as it was found in Ref. [25].

substrate are summarized in Fig. 7. Three samples, 1×100, 2×50, and 3×50, are exactly those which were used for the terahertz spectroscopic experiments. The two other samples, 4×50B and 4×50C, were characterized only by XRD. In this figure one of the in-plane constants and the out-of-plane lattice constant of these STO films are presented. We show STO in-plane lattice constants oriented along the [1$\bar{1}$ 0] DSO crystallographic direction constituting the shorter constant of a pseudosquare surface mesh of (110) DSO. The surface mesh is formed by spacings of 3.948 and 3.951 Å. These values are calculated using the substrate lattice constants determined from our XRD experiments: $a = 5.443 \pm 0.005$ Å, $b = 5.720 \pm 0.0025$ Å, and $c = 7.902 \pm 0.0005$ Å. These parameters agree well with previous data [7,21–23], taking into account the fact that the slight difference in lattice constants may be observed due to intrinsic defects [23] coming from small deviations in stoichiometry [21].

As it was expected, sample 2×50 possesses a more expanded (i.e., closer to that of DSO substrate) in-plane lattice constant than sample 1×100 (see Fig. 7). This actually correlates with the observed temperature behavior of the soft mode in these structures.

It has been shown [24,25] that the out-of-plane lattice constant of STO thin films possesses the lowest value for

TABLE II. Summary of the evaluated characteristics of the thin-film structures. The soft-mode frequency ω_0 and the permittivities ε_0 and $\varepsilon_{0.5}$ for 0 kV/cm and their change upon 67 kV/cm ($\Delta\omega_0$, $\Delta\varepsilon_0$, $\Delta\varepsilon_{0.5}$) were taken at T_C for most samples. The static permittivity value ε_0 and its value at 0.5 THz, $\varepsilon_{0.5}$, were evaluated using parameters obtained from the fits. SC denotes single crystal of $SrTiO_3$.

Sample	1×100	2×50	3×50	$4 \times 50 \times 2$	4×50A	6×50	8×50	20×10[a]	SC[b]
d_{STO} (nm)	100	100	150	200[c]	200	300	400	200	–
$\omega_0(0)$ (cm^{-1})	39.5	46.6	54	51.1	47	48	59.1	65	38.5
$\Delta\omega_0(67)$ (cm^{-1})	21.3	21.4	10.9	8.1	15.5	8.7	6.6	5	10.5
$\varepsilon_0(0)$	4600	2010	1420	1760	2700	2050	1370	1050	1590
$\Delta\varepsilon_0(67)$	3920	1380	440	600	1650	720	330	150	610
$\varepsilon_{0.5}(0)$	880	770	960	1000	1030	930	780	750	1950
$\Delta\varepsilon_{0.5}(67)$	470	290	200	170	250	70	120	50	840
T_C (K)	250	294[d]	275	275	275	250	275	225	–
f (10^6 cm^{-2})					2.36				2.34
Γ (cm^{-1})[e]	55	57	48	69	48	79	77	92	5.2
γ (cm^{-1})	6–23	7–30	10–17	6–15	10	7–23	17–20	10	–
δ (cm^{-1})	32	33	28	32	35	33	32	34	–
β (10^9 $JC^{-4}m^5$)	8.6	18	19	11	14	5.2	8.2	9	0.8
c (Å)	3.8894	3.886	3.8868		3.8894 3.8861[f]				3.905

[a]The data for this sample are taken from Ref. [10], and they are available only for 294 K (not T_C).
[b]The data obtained at 90 K (not T_C).
[c]Despite the overall STO thickness of 400 nm in this structure, only a 200-nm-thick part of STO was influenced by the bias electric field.
[d] The probable value of T_C for the 2×50 sample in the range 290–310 K (determined by extrapolation only).
[e]The data are taken at T_C.
[f]These values are measured on nominally the same (4×50B and 4×50C) structures as 4×50A.

nominally stoichiometric films, and it increases in samples with a small deviation in the stoichiometry. This has been explained by the presence of defects originating from off-stoichiometric composition of the film [25]. In our case, we can assume that the sample preparation conditions by PLD were kept very similar for the studied samples. This assumption is very close to reality, at least for samples 1×100, 2×50, and 3×50, which were prepared in a single series. Therefore differences in the out-of-plane lattice constants among these samples indicate the defect concentration and consequently, the degree of epitaxial strain relaxation in the thin-film structures. Again, sample 2×50 is more perfect than 1×100 from this point of view. Sample 3×50 has more defects than 2×50 but still less than 1×100. It means that despite an increase of the total STO thickness compared to sample 1×100, this structure possesses a less expanded out-of-plane lattice constant and an in-plane lattice constant closer to that of the substrate (see Fig. 7). The values of the out-of-plane lattice constant are summarized as well in Table II.

As it was already mentioned, samples 4×50B and 4×50C were deposited in a single series. Therefore the differences in the structural parameters of these thin-film structures provide us with an approximate uncertainty due to the preparation process. In addition, we can roughly compare these samples with the others. From Fig. 7 one can see that even these structures with four 50-nm-thick STO layers are better from a structural point of view than a single 100-nm-thick layer of STO.

Despite the significant strain relaxation in the relatively thick STO layer, the 1×100 structure shows the lowest soft-mode frequency (39.5 cm^{-1}) among the others. The 2×50 structure acquires also a low minimum value of the soft-mode frequency, especially if one considers its possible further softening with a small temperature increase. The structures with more than two layers of STO exhibit slightly higher soft-mode frequencies at the phase transition temperature T_C. This fact can be connected again to an inhomogeneous distribution of the strain over the multilayer structure thickness, which eventually results in slightly different lattice dynamics in the individual STO layers within one multilayer structure.

The 1×100 and 6×50 samples exhibit the lowest phase transition temperature (250 K). At the same time, we obtained a significantly larger value of the relaxation strength g for these structures than for the others (with the exception of 8×50 sample). This fact might be connected to a higher concentration of defects within these heterostructures. It has been shown [13] that the epitaxial strain relaxes on defects. Then partially relaxed epitaxial strain might be a reason for a lower T_C observed in these structures.

Recently, qualitatively the same picture was observed during the study [25] of a stoichiometric effect on the dielectric properties and soft-mode behavior of strained 50-nm-thick single STO layers on DSO substrates. In that work, the nominally stoichiometric sample was found to undergo the phase transition temperature at ~300 K, while thin films with a slightly off-stoichiometric composition experience the phase transition at lower temperatures. It was concluded that defects coming from a weak off-stoichiometry of the composition favor the epitaxial strain relaxation. Consequently, this leads to the decrease of the phase transition temperature observed for the nonstoichiometric thin films. Note that the anomaly of the soft-mode frequency at the phase transition of the stoichiometric sample was sharp and deep (softening down to ~20 cm^{-1}) [25], while the soft-mode minima observed in samples studied in this work

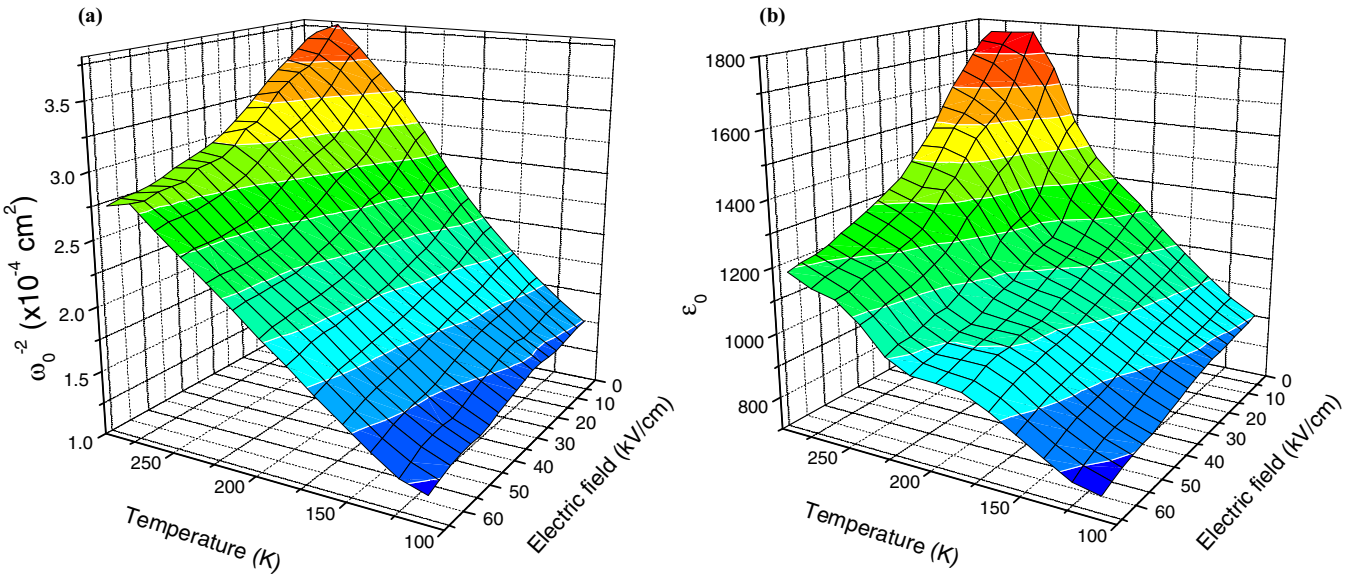

FIG. 8. (Color online) Temperature and electric-field dependence of (a) squared inverse soft-mode frequency as obtained from the fits, and (b) static permittivity obtained by extrapolation of the dielectric spectra using fitted parameters. White lines are contour lines corresponding to major and minor ticks on the z axes. Data obtained on a $4 \times 50 \times 2$ sample.

greatly resemble those obtained for slightly off-stoichiometric samples.

The soft-mode damping acquired different values from sample to sample, which were, however, in the range between 43 and 90 cm^{-1}. We observe a general tendency of an increase of Γ for thicker samples. The damping value of each sample did not vary more than by 50% with temperature, but no clear trend in the temperature dependence was observed. In our fits we assumed that Γ is electric-field independent. The thin-film structures with a higher number ($\geq$6) of individual STO layers exhibit slightly larger values of the soft-mode damping and of its variation with temperature (see Table II).

B. Relaxation

We did not need to introduce an electric-field dependence of the relaxation frequency in order to fit the spectra. However, the relaxation frequency was found to depend on temperature in the second step of fitting. The values also slightly varied from sample to sample. The obtained ranges of relaxation frequency for each sample are presented in Table II; the reported variation versus temperature was observed mainly at low temperatures ($T \lesssim 120K$). At high temperatures (>180 K) the form of the experimental terahertz spectra is mainly given by the soft-mode contribution to the permittivity and only the lower-frequency part of the spectra is influenced by the relaxation thanks to its coupling to the soft mode. At low temperatures ($\leq$120 K) the soft mode lies above the accessible spectral range and its contribution to the spectra virtually consists of a quasiconstant background; the shape of the spectra is completely governed by the relaxation mode. This is clearly illustrated by green and blue data points in Fig. 2 corresponding to 20 and 120 K, respectively. These data constitute an unambiguous proof of the existence of the central mode at low temperatures and of its polar character (direct coupling to the polarization independently of the soft mode). Generally, the relaxation shows a gradual increase of its frequency on cooling within the range shown in Table II. Small deviations of the best fit from the experimental dielectric spectra observed in some cases at low temperatures suggest that in reality there might be several relaxation processes with a distribution of their frequencies within the strained films.

In Fig. 8 we show temperature and electric-field dependences of squared inverse soft-mode frequency $\omega_0^{-2}(T,E)$ [Fig. 8(a)] and of the extrapolated static permittivity $\varepsilon_0(T,E)$ calculated using our model [Fig. 8(b)]. The data are obtained with a $4 \times 50 \times 2$ thin-film heterostructure. In the case of single crystals of STO, where the soft mode contribution to dc permittivity is dominant (about 96%), and according to the Lyddane-Sachs-Teller relation implying $\varepsilon_0 \propto \omega_0^{-2}$, one could expect qualitatively similar pictures in the corresponding graphs. However, in our plots we do observe marked differences. Evidently, $\varepsilon_0(T,E)$ includes not only the contribution from the ferroelectric soft mode, but also contributions from other excitations. At high temperatures ($\geq$220 K), where the soft-mode frequency is low, the leading extra dielectric contribution comes from the silent coupled relaxation mode.

The relaxation strength acquires nonzero values only in the ferroelectric phase of the STO films, as it was mentioned above [see inset in Fig. 5(a)]. We point out that at lower temperatures the relaxation mode is much stronger in 1×100, 6×50, and 8×50 samples (in which substantial epitaxial strain relaxation occurs) than in the others. As a result, the low-frequency permittivity maintains high values even at the lowest temperatures due to the relaxation contribution to the terahertz permittivity.

The coupling constant exhibits similar values ($\delta \approx 32\,\text{cm}^{-1}$) for all samples; the values are summarized in Table II. This means that the oscillator-relaxator coupling is universal near the ferroelectric phase transition and below, and it does not depend on the magnitude of the strain.

An extensive discussion has been recently carried out, supported by a comparison between experimental spectroscopic results and effective Hamiltonian-based molecular dynamics simulations, about the existence and origin of the central mode in the (Ba,Sr)TiO_3 (BST) family of perovskite ferroelectrics [26–28]. In Ba-rich BST compounds, a strong central mode appears in a broad range of temperatures above the ferroelectric phase transition and it has been shown to be connected to the soft-mode eigenvector [26,27], i.e., it is of intrinsic origin and it arises from the complexity of the soft-mode potential. Simulations carried out on $BaTiO_3$ suggested that the mode originates in the hopping between the soft-mode potential minima [28]. For Sr-rich BST materials the temperature range of existence of the central mode gets narrower, and finally, the central mode does not appear in the spectra of a pure STO single crystal [5,27,29]. However, as shown experimentally in this work and also suggested recently by effective Hamiltonian simulations [29], upon application of a tensile strain, the central mode does appear in the in-plane GHz-THz response in STO thin films. A semiquantitative agreement between the theory and experiment lead us to the conclusion that in our strained samples the relaxation should be a consequence of the complex landscape of the soft-mode potential at least in the vicinity of the ferroelectric phase transition. At low temperatures the central mode is strengthened in our experiments, despite an appreciable hardening of the soft mode; the bilinear coupling between these two modes ceases to be significant. This may suggest a change in the character of the relaxation at low temperatures.

C. Anharmonic behavior

In order to analyze the dielectric tunability of the samples we compared the static permittivity values ε_0 obtained at 0 and at 67 kV/cm bias. These values were calculated by extrapolation of the model with the fitted parameters to the zero frequency. We emphasize that these values should be understood as terahertz data extrapolations and they have a good meaning only for our comparison. They should not be considered as approximations of "true" static values, because other low-frequency excitations, which may significantly contribute to the permittivity (for example, a contribution due to the domain walls), are also expected to appear in the ferroelectric phase. The extrapolated static permittivity values ε_0 are shown in Table II together with the permittivity values $\varepsilon_{0.5}$ obtained by the fits at 0.5 THz under the same applied electric fields. First, from a comparison of ε_0 and $\varepsilon_{0.5}$ values it is seen that the relaxation-mode contribution to the permittivity is substantial. Second, the tunability strongly correlates with the soft-mode frequency: a lower soft-mode frequency implies a stronger field-induced change in the permittivity. This trend manifests both in the behavior of the extrapolated static permittivity and of the permittivity found at 0.5 THz, regardless of the contribution given by the relaxation mode.

One can also observe two mutually coupled general tendencies: the minimum value of the soft-mode frequency found at the phase transition temperature (shown in Table II) increases with an increase in the number of STO/DSO bilayers in the structures, while a decrease in tunability of the soft-mode frequency and, consequently, in tunability of the permittivity is observed.

To interpret the electric-field-induced soft-mode behavior, we consider the model developed in Ref. [11], where it is assumed that thanks to the interdigitated electrode structure deposited on the samples, we applied relatively high electric fields which may pole STO films in the ferroelectric phase and induce regions with a nonvanishing macroscopic polarization in between electrode fingers. The soft-mode frequency ω_0 then changes not only due to the applied bias electric field E, but it is also renormalized by the spontaneous polarization value P_s. In the weak-field limit the field-induced soft-mode hardening is then expressed in the following way [11]:

$$\omega_0(T,E) = \omega_0(T,0)\sqrt{1 + 3\beta\left[\varepsilon_{\text{vac}} f/\omega_0^2(T,0)\right]^3 E^2 + 6\beta\left[\varepsilon_{\text{vac}} f/\omega_0^2(T,0)\right]^2 P_s E}, \quad (5)$$

where β is the coefficient that characterizes the fourth-order anharmonicity of the soft-mode potential minimum [11] and ε_{vac} is the vacuum permittivity. The system of interdigitated electrodes implies that the adjacent gaps between the electrode fingers are poled with opposite field. This means that while the sign of P_s alternates in the adjacent gaps, the mixed term $P_s \cdot E$ in Eq. (5) should be positive in each gap and contributes to the electric-field-induced soft-mode hardening. Note that Eq. (5) was derived under the assumption of a silent relaxation mode and becomes an approximation at low temperatures where the morphic relaxation strength g becomes non-negligible. However, taking into account the accuracy of our determination of the soft-mode and relaxation-mode parameters, we still keep it for evaluations down to 120 K.

The experimentally obtained electric-field dependencies of the soft mode in each sample were fit by Eq. (5) in the ferroelectric phase and $P_s = 0$ was assumed in Eq. (5) for the paraelectric phase. Fits for the 6×50 sample are shown in Fig. 6. They describe well two basic features observed in the figure: (i) the soft-mode tunability does not substantially decrease with decreasing temperature below the phase transition, as would be expected from the observed soft-mode hardening $\omega_0(T)$; (ii) at low temperatures the variation of $\omega_0(T,E)$ with field tends to be linear even for low applied fields. Both these phenomena are explained by the nonvanishing spontaneous polarization P_s in the ferroelectric phase.

At temperatures of the phase transition or higher, i.e., where $P_s = 0$, the only fitting parameter in Eq. (5) is the anharmonic coefficient β. The fitted values of β are presented in Table II. In the weak-field limit ($E < 35$ kV/cm), the soft mode exhibits a quadratic growth with external bias (Fig. 6). At temperatures below the phase transition, we assumed that β is a temperature-independent parameter. We used the values found by fitting the soft-mode tunability in the paraelectric

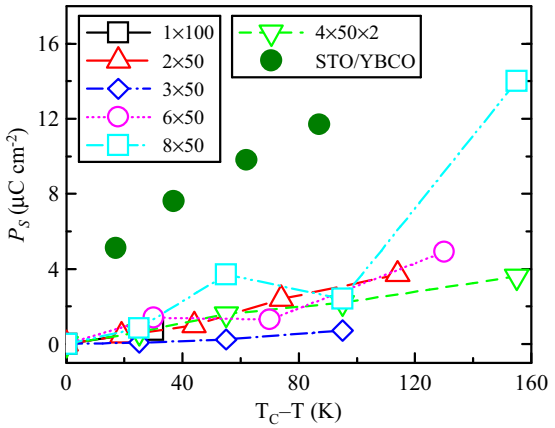

FIG. 9. (Color online) Estimated temperature dependence of the spontaneous polarization. Empty symbols are values obtained by the fits of our data. Lines are guides to the eye. Solid symbols are polarization values found in the literature for thin films of $SrTiO_3$ deposited on a bulk $SrTiO_3$ with an intercalated $YBa_2Cu_3O_{7-x}$ electrode layer [30].

phase (shown in Table II) for fitting the soft-mode behavior in the ferroelectric phase. The spontaneous polarization P_s was again the only fitting parameter in the model. An increase of its value was observed on cooling. The temperature dependence of the spontaneous polarization for the investigated samples is shown in Fig. 9. These values should be considered with caution, because a possible contribution of higher-order terms in Eq. (5) cannot be excluded within the accuracy of our experimental data and, in reality, the anharmonic coefficient β can exhibit weak temperature dependence, as it was found for STO single crystals [5]. Nevertheless, we think that the values of the spontaneous polarization found in the framework of our approach (Fig. 9) are quite reasonable. Our values are of the same order of magnitude as those reported previously for a thin film of STO on bulk $SrTiO_3$ with a $YBa_2Cu_3O_{7-x}$ interlayer [30]. The data from the literature are shown together with ours in Fig. 9.

VI. CONCLUSION

We characterized the terahertz dielectric properties and the electric-field tunability of several STO/DSO thin-film structures using the time-domain terahertz spectroscopy and x-ray diffraction. The dielectric spectra were obtained in a broad temperature range (20–294 K), which allowed us to estimate the paraelectric-to-ferroelectric phase transition temperatures for all the investigated structures. A general model for the terahertz permittivity was shown to describe well all the measured spectra at different temperatures and applied electric fields. The model includes a damped harmonic oscillator (soft mode) coupled with a Debye relaxation (central mode). The variation of the soft-mode frequency with temperature and electric field $\omega_0(T,E)$ is demonstrated to be responsible for the general evolution of the terahertz spectra. At higher temperatures the central mode significantly contributes to the low-frequency part of the spectra, whereas it fully determines the observed spectral shape at temperatures below 120 K.

Unexpectedly, the electric-field tunability does not substantially decrease with cooling below the phase transition temperature. We explained this by a high value of the spontaneous polarization, which renormalizes the effective potential of the soft mode.

The observed variation of the phase transition temperature and of the terahertz dielectric response among the structures is ascribed to a partial strain relaxation with increasing total STO thickness. The epitaxial strain relaxation is confirmed by XRD experiments. Nevertheless, the structures with a high number of STO/DSO bilayers ($\geq$6) still undergo the phase transition, confirming that our approach to maintain STO layers strained by sequential intercalation of thin DSO layers is valid.

Taking into account all the experimental data and their complete analysis, we can state that the most optimal structure for the tunable applications is the one possessing four STO/DSO bilayers. It has a total STO thickness of 200 nm and exhibits a comparatively high tunability which is not deteriorated by a strongly pronounced relaxation. In addition, a functional structure can be prepared with the thin-film structure on both sides.

ACKNOWLEDGMENTS

This work was supported by the Czech Science Foundation (Project No. 14-25639S) and by European Union funding under the 7th Framework Programme (Project NOTEDEV).

[1] M. E. Lines and A. M. Glass, *Principles and Applications of Ferroelectrics and Related Materials* (Clarendon Press, Oxford, 1979).
[2] K. A. Muller and H. Burkard, Phys. Rev. B **19**, 3593 (1979).
[3] H.-M. Christen, J. Mannhart, E. J. Williams, and Ch. Gerber, Phys. Rev. B **49**, 12095 (1994).
[4] A. Eriksson, A. Deleniv, and S. Gevorgian, J. Appl. Phys. **93**, 2848 (2003).
[5] V. Skoromets, F. Kadlec, C. Kadlec, H. Němec, I. Rychetsky, G. Panaitov, V. Müller, D. Fattakhova-Rohlfing, P. Moch, and P. Kužel, Phys. Rev. B **84**, 174121 (2011).
[6] A. K. Tagantsev, V. O. Sherman, K. F. Astafiev, J. Venkatesh, and N. Setter, J. Electroceram. **11**, 5 (2003).
[7] J. H. Haeni, P. Irvin, W. Chang, R. Uecker, P. Reiche, Y. L. Li, S. Choudhury, W. Tian, M. E. Hawley, B. Craigo, A. K. Tagantsev, X. Q. Pan, S. K. Streiffer, L. Q. Chen, S. W. Kirchoefer, J. Levy, and D. G. Schlom, Nature (London) **430**, 758 (2004).
[8] P. Kužel, F. Kadlec, J. Petzelt, J. Schubert, and G. Panaitov, Appl. Phys. Lett. **91**, 232911 (2007).
[9] P. Kužel, C. Kadlec, F. Kadlec, J. Schubert, and G. Panaitov, Appl. Phys. Lett. **93**, 052910 (2008).

[10] C. Kadlec, F. Kadlec, H. Němec, P. Kužel, J. Schubert, and G. Panaitov, J. Phys.: Condens. Matter **21**, 115902 (2009).
[11] C. Kadlec, V. Skoromets, F. Kadlec, H. Němec, J. Hlinka, J. Schubert, G. Panaitov, and P. Kužel, Phys. Rev. B **80**, 174116 (2009).
[12] W. Chang, J. A. Bellotti, S. W. Kirchoefer, and J. M. Pond, J. Electroceram. **17**, 487 (2006).
[13] Z. Y. Zhai, X. S. Wu, H. L. Cai, X. M. Lu, J. H. Hao, J. Gao, W. S. Tan, Q. J. Jia, H. H. Wang, and Y. Z. Wang, J. Phys. D: Appl. Phys. **42**, 105307 (2009).
[14] P. Kužel, H. Němec, F. Kadlec, and C. Kadlec, Opt. Express **18**, 15338 (2010).
[15] F. L. Pedrotti and L. S. Pedrotti, *Introduction to Optics*, 2nd ed. (Prentice Hall, Upper Saddle River, NJ, 1993), Chap. 19, pp. 392–404.
[16] A. S. Barker and J. J. Hopfield, Phys. Rev. **135**, A1732 (1964).
[17] Y. Girshberg and Y. Yacoby, Solid State Commun. **103**, 425 (1997).
[18] V. Skoromets, S. Glinšek, V. Bovtun, M. Kempa, J. Petzelt, S. Kamba, B. Malič, M. Kosec, and P. Kužel, Appl. Phys. Lett. **99**, 052908 (2011).
[19] P. Kužel and F. Kadlec, C. R. Physique **9**, 197 (2008).
[20] J. Hemberger, P. Lunkenheimer, R. Viana, R. Böhmer, and A. Loidl, Phys. Rev. B **52**, 13159 (1995).
[21] M. D. Biegalski, D. D. Fong, J. A. Eastman, P. H. Fuoss, S. K. Streiffer, T. Heeg, J. Schubert, W. Tian, C. T. Nelson, X. Q. Pan, M. E. Hawley, M. Bernhagen, P. Reiche, R. Uecker, S. Troiler-Mckinstry, and D. G. Schlom, J. Appl. Phys. **104**, 114109 (2008).
[22] J. E. Kleibeuker, D. Kuiper, S. Harkema, D. H. A. Blank, G. Koster, G. Rijnders, P. Tinnemans, E. Vlieg, P. B. Rossen, W. Siemons, G. Portale, J. Ravichandran, J. M. Szepieniec, and R. Ramesh, Phys. Rev. B **85**, 165413 (2012).
[23] M. Schmidbauer, A. Kwasniewski, and J. Schwarzkopf, Acta Crystallogr., Sect. B **68**, 8 (2012).
[24] C. M. Brooks, L. F. Kourkoutis, T. Heeg, J. Schubert, D. A. Muller, and D. G. Schlom, Appl. Phys. Lett. **94**, 162905 (2009).
[25] C.-H. Lee, V. Skoromets, M. D. Biegalski, S. Lei, R. Haislmaier, M. Bernhagen, R. Uecker, X. Xi, V. Gopalan, X. Martí, S. Kamba, P. Kužel, and D. G. Schlom, Appl. Phys. Lett. **102**, 082905 (2013).
[26] I. Ponomareva, L. Bellaiche, T. Ostapchuk, J. Hlinka, and J. Petzelt, Phys. Rev. B **77**, 012102 (2008).
[27] J. Weerasinghe, L. Bellaiche, T. Ostapchuk, P. Kužel, C. Kadlec, S. Lisenkov, I. Ponomareva, and J. Hlinka, MRS Commun. **3**, 41 (2013).
[28] J. Hlinka, T. Ostapchuk, D. Nuzhnyy, J. Petzelt, P. Kužel, C. Kadlec, P. Vaněk, I. Ponomareva, and L. Bellaiche, Phys. Rev. Lett. **101**, 167402 (2008).
[29] J. Weerasinghe, D. Wang, and L. Bellaiche, J. Phys.: Condens. Matter **25**, 252202 (2013).
[30] D. Fuchs, C. W. Schneider, R. Schneider, and H. Rietschel, J. Appl. Phys. **85**, 7362 (1999).